Segmentation of gray scale images of dropwise condensation on textured surfaces

Helene Martin, Solmaz Boroomandi Barati, Nicolas Pionnier, Jean-Charles Pinoli, Stephane Valette, and Yann Gavet,

Abstract—In the present work we developed an image processing algorithm to measure water droplets characteristics during dropwise condensation on pillared surfaces. The main problem in this process is the similarity between shape and size of water droplets and the pillars. The developed method divides droplets into four main groups based on their size and applies the corresponding algorithm to segment each group. These algorithms generate binary images of droplets based on both their geometrical and intensity properties. The information related to droplets evolution during time including mean radius and drops number per unit area are then extracted from the binary images. The developed image processing algorithm is verified using manual detection and applied to two different sets of images corresponding to two kinds of pillared surfaces.

Keywords—Dropwise condensation, textured surface, image processing, watershed.

I. Introduction

DROPWISE condensation attracted lots of attention in many industrial applications since about 80 years ago [1] due to its high rate of heat transfer [2]. Though this phenomenon is not preferred in optical applications, for example in automotive industry the light passing through car headlights distracts by water droplets generated during dropwise condensation.

Generally condensation occurs when the temperature of saturated air goes behind its dew point [3]. In this case, water droplets start to nucleate either in the air mixture or on the cold substrate of chamber walls. Regarding condensation on cold substrate, nucleation can occur homogeneously (when there is no preference between different spots for nucleation) or heterogeneously (preferentially on the surface imperfections) [4]. In both cases, dropwise condensation occurs in four main steps: nucleation, growth of droplets by adsorbing water molecule, coalescence and steady state. In the last step, a constant pattern in both the size and number of droplets is visible [5].

Heterogeneous dropwise condensation on textured surfaces is now more attractive to scientists because of the ability of controlling droplets configuration [6]. This idea could also be interesting for optical applications. Indeed, this solution could make drops to form a continuous film or to drain quickly from the surface of headlights or glasses. Thus, several techniques were developed in order to study the characteristics and the evolution of droplets on textured surfaces. The first step of all these methods is the image processing techniques that extract all droplets information from gray scale images. These techniques deal with non intrusive methods with a high spatial and temporal resolution [7].

Most of the time, such image processing algorithms are divided into three main steps: pre-processing, drop segmentation and drop reconstruction. The first one aims at improving contrast and removing noise in order to facilitate the drop segmentation step. The drop segmentation step consists of isolating drops from the background and then separating overlapping drops. The corresponding algorithms can be classified into three groups: the ones based on the shape analysis, based on the edge analysis, and based on the intensity analysis. The algorithms based on the shape analysis consider drops as circles with dark edges and bright centers. These drops can be detected by using circle detection methods like the Hough transform [8] and its improvements, such as the normal-line Hough transform [9] and the coherent circle Hough transform [10]. However, these methods are only efficient for spherical droplets. The algorithms based on the edge analysis use images generated by an edge detection method [11]. For this purpose, the Canny method seems to be the most convenient since although it is more sensitive to noise with respect to other methods, it provides more connected contours. Then the contour discontinuities that represent multiple drops overlapping are detected. such points are called breakpoints, that can be detected by means of several techniques, either by rotating the edge curves [12] or by analyzing their curvature [13], [14]. The main drawback of these techniques is the noise sensitivity, which necessitates to smooth the edge curvatures. A way to limit the noise sensitivity of measurements is to use an

H. Martin is with Ecole Nationale Suprieure des Mines de Saint-Etienne, LGF UMR CNRS 5307, SAINT-ETIENNE, France.

S. Boroomandi Barati is with Univ Lyon, Ecole Nationale Suprieure des Mines de Saint-Etienne, LGF UMR CNRS 5307, SAINT-ETIENNE, France,e-mail: (solmaz.boroomandi@emse.fr).

N. Pionnier is with Univ Lyon, Ecole Centrale de Lyon, LTDS UMR CNRS 5513, F-69134, LYON, France

J.-C. Pinoli is with Ecole Nationale Suprieure des Mines de Saint-Etienne, LGF UMR CNRS 5307, SAINT-ETIENNE, France.

S. Valette is with Univ Lyon, Ecole Centrale de Lyon, LTDS UMR CNRS 5513, F-69134, LYON, France

Y. Gavet is with Ecole Nationale Suprieure des Mines de Saint-Etienne, LGF UMR CNRS 5307, SAINT-ETIENNE, France.

adaptive curvature [15]. Finally, the algorithms based on an intensity analysis use the gray-level intensities as a drop presence indicator. These intensities can be used directly like the PIV methods [16] using a dynamic thresholding and watershed [17] or indirectly like the appearance-based approaches using an isolated drop to select the same appearance drops [18]. These methods can be combined thorough a tree of decision to improve the detection quality [7]. For instance, the PIV methods are particularly efficient for isolated drops while the watershed method works well for overlapping ones. However, this combination requires a long computational time.

The drop reconstruction step consists of reconstructing missing parts of drops by determining their radius and their centers. These methods can be divided into four main groups: the ones based on ellipse fitting, based on the geometrical analysis, based on the morphological analysis and the ones using drop inner boundaries. The ellipse fitting methods consist of recognizing ellipse-like shapes in the image. For this purpose, least-squares fitting methods [19] or k-means methods [20] are used. However, these methods work only on ellipsoidal droplets. The geometrical methods aim at determining whether two arcs belong to the same drops by means of either correlation coefficients [12] or applying convexity criteria directly to the contour image [21] or to the polygonal approximation image [22]. The main drawback of these methods is the use of deterministic parameters. The morphological techniques use the morphological reconstruction principle. For this purpose, overlapping drops are reduced to independent characteristic areas before being reconstructed, but the percentage of overlapping droplets must not be too high. Different techniques can be used in this regard: successive erosion [23], [24], skeletonization and shrinking [25] or the watershed technique applied to a distance map [26]. After all, a final technique is applied in order to complete missing parts of droplets by using drops inner boundaries [7]. This last method necessitates high inner boundaries quality.

However, in the case of textured surfaces, the pillars which represent the texturation do not let one to use directly these techniques, although they are adapted to different drop shapes and image conditions. Indeed, pillars have the same properties as drops, they have dark edges and bright centers. Moreover, when the drop shape becomes irregularly connected over the pillars, the already-existing methods are not able to separate them and recognize each droplet. Thus, the goal of this work is to find a way to detect separately drops and pillars in order to analyze drop characteristics evolution on the surface.

This work consists of finding an automatic way to segment drops on several textured surfaces in order to study droplets characteristics. In the following, the experimental set-up enabling to photograph textured surface under dropwise condensation condition will be described. Then, the details of the developed image processing algorithm will be presented. Finally, the algorithm accuracy will be determined and the measurement results will be discussed.

II. Experimental set-up

The schematic of the experimental set-up is shown in figure 1. The textured substrate with temperature 281K is placed inside a humid chamber with relative humidity of about 40% and air temperature of 303K. The humid air is generated by mixing filtered compressed air and saturated air.

Dropwise condensation on the sample is recorded by a CCD gray scale camera at each second. This camera uses a long-focal-distance adjustable lens in order to get a high spatial resolution. The gray-level images are then used in the following image processing algorithm.

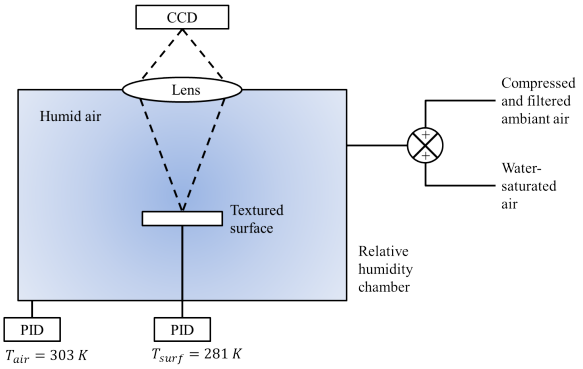

Fig. 1. Schematic of the experimental set-up

III. Image processing algorithm

An image processing algorithm has been developed to segment drops and to analyze drop characteristic evolution during dropwise condensation. This algorithm is applied to a set of images and it consists of three main steps as shown in figure 2. The pillar characterization step aims at isolating pillars in order to remove them from the other images. The goal of the second step is to divide the image set into several groups: very small drops, small drops, medium drops and big drops. The first two groups refer to the drop growth by adsorption. The third group corresponds to the coalescence step and the last one corresponds to the steady state where the changes in size and number of droplets are negligible. After this categorization, the corresponding image processing algorithm is applied to each group. Thus, an image of drop segmentation is generated on which the mean radius and drop number can be measured.

A. pillar characterization

The goal of this step is to isolate pillars from background in order to remove them in the other images. In fact, pillars can entail mis-measurement because of

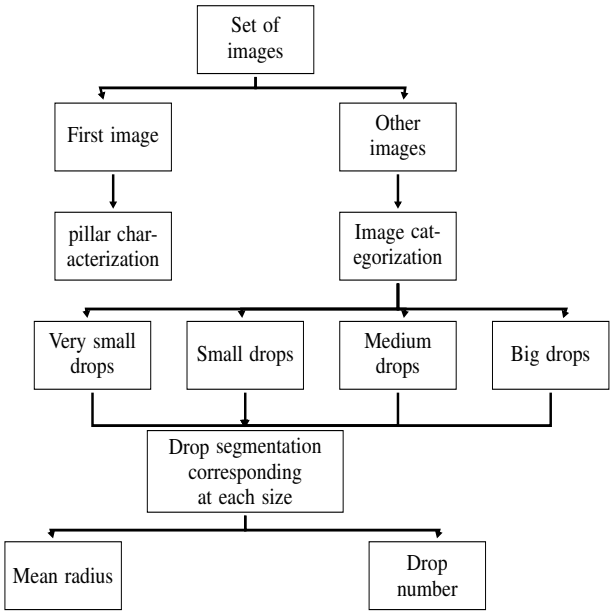

Fig. 2. Schematic diagram of the image processing algorithm

their similar properties to drops. As the images are taken without shifting, pillars are at the same location on the images from the same set. So for the purpose of pillar elimination, the first image of the considering set is used because the drop presence can be neglected. The algorithm is detailed in figure 3.

As pillars are perfectly circular, the circle Hough transform is the most adapted technique. Moreover, an approximation of pillar radius is known. Indeed, their real size is between 10 and 20 μm and according to the camera magnification, the radius range considered for the Hough transform is [10; 30] pixels. It is important to consider a quite narrow range in order to get accurate results and a low computational time. To improve again the algorithm performances, the coherent Hough transform is used [10].

By means of this method, all the pillars are detected except the ones at the image borders. However, some artefacts are detected too as shown in figure 3 (b). As they don't have the same size as pillars, a technique to solve this problem is to consider the distribution of circle radius and to remove the ones with an aberrant radius, as shown in figure 3 (c) and (d). Thus, the circle radius must be inside the band [μ - 3.9 σ; μ + 3.9 σ] to be considered as pillars, where μ and σ are the average and the standard deviation of the radius distribution.

At the same time, a manual pillar recognition test is led, as shown in figure 3 (e). This secondary method enables to confirm the position of pillars and to validate the calculated radius. Indeed, if the radius are smaller than the real ones, the pillar boundaries will not be taken into account and they will be considered as pillars during the drop segmentation step. Similarly, if the radius are wider than the real ones, some drops will be removed.

Figure 3 (f) shows that pillars from the Hough transform are lightly smaller than the real ones, that can be explained by their blurred boundaries. Consequently, the circles from the Hough transform must be enlarged. In order to quantify the correct radius, the equivalent circle radius is calculated by means of the manual measurements. This equivalent radius refers to the radius of the circle with the same center as the one from the Hough transform but covering both the Hough transform circle and the manual measured circle, as shown in figure 4. In our case, pillar radius must be enlarged from four-pixel wide.

Finally, the binary image of the pillars is generated. The image with the radius from the Hough transform is firstly generated and then, the image is dilated by a disk structuring element, whose radius corresponds to circle enlargement found previously. The final results show visually good approximation of the pillar location and dimension.

It is important to note that the pillars close to the image borders can't be detected because the missing parts are too large. Thus, this problem must be taken into account in the next parts of the algorithm. For instance, the images will be resized.

B. Image categorization

As mentioned previously, there are four kinds of drops: very small drops, small drops, medium drops and big drops. It is important to distinguish these groups because the drop identification algorithm will be adapted to each kinds of drops.

This step is like a texturation determination process. Two main categorization methods exist: the ones based on the intensity distribution [27] and the ones based on the pattern distribution [28], [29]. As the image categorization needs to be very fast, the study of intensity histograms is more preferred in our case.

Firstly, a sub-sampling of the image set is done to limit the computational time. Thus, ten percent of images have been chosen regularly, since the time step between images is equal to 1s, 10% of images means the images have been taken after each 10s. The corresponding gray-tone level histograms of each studied image is determined. As shown in figure 5, the number of major peaks in histograms vary as a function of time. This variation represents the different drop sizes. Thus, the ranges of each size group of drops are characterized:

- Very small drops: histogram with three major peaks, corresponding to the background, the drop edge and the drop center.
- Small drops: after a while when the histogram of gray tone turns in to bimodal diagram, the majority of droplets are called small droplets that grow mainly due to adsorption. With respect to the former stage

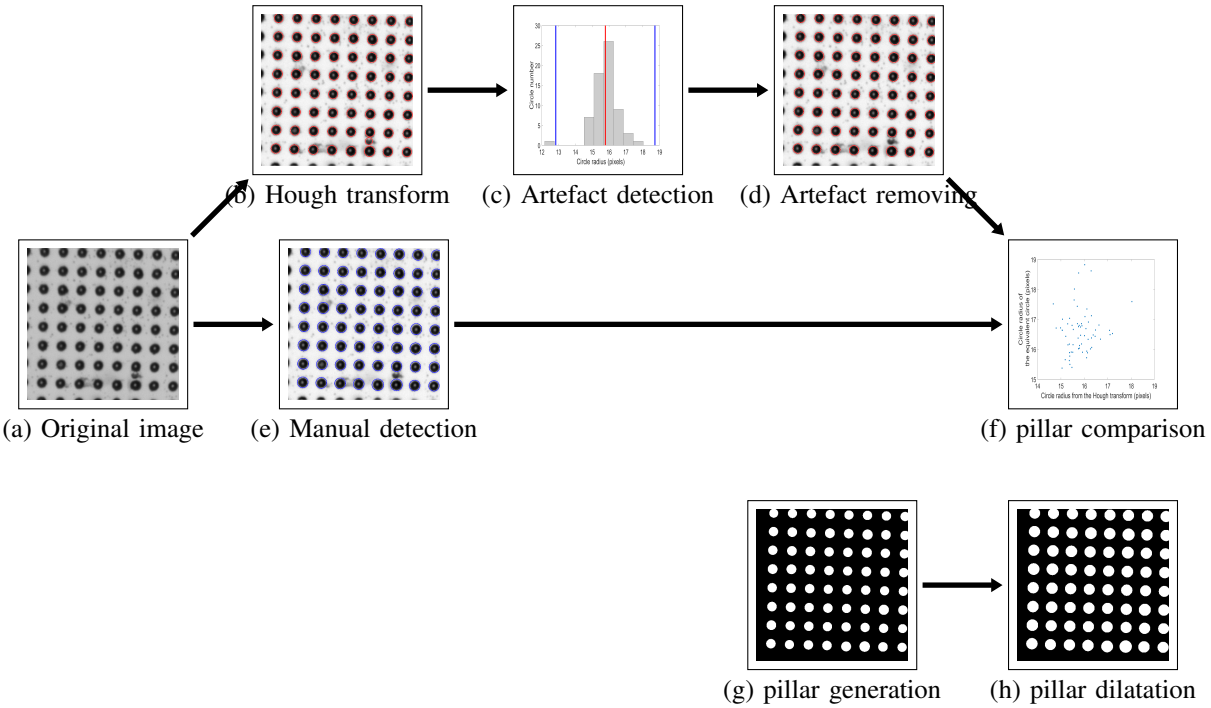

Fig. 3. Algorithm for pillar characterization

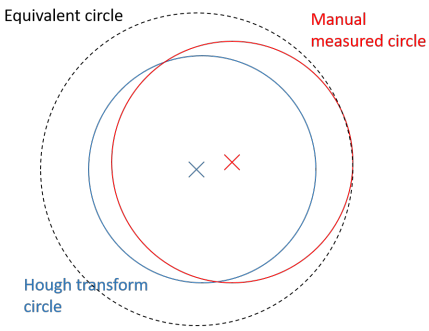

Fig. 4. Equivalent circle determination

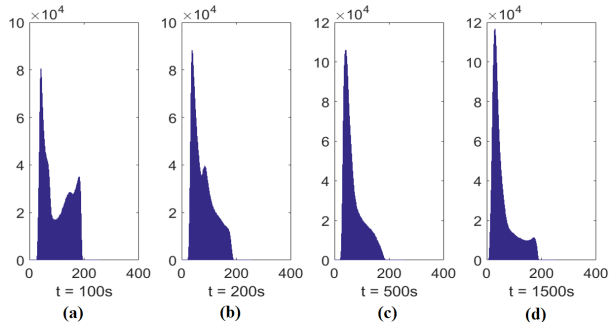

Fig. 5. Intensity histogram of (a) very small droplets at t = 100s, (b) small droplets at t = 200s, (c) medium droplets at t = 500s and (d) big droplets drops at t = 1500s.

here the peak related to the background disappeared because drops tend to cover entirely the sample.

- Medium drops: In the third stage, drops start to coalesce and their centers become larger with the same intensity as background. Therefore the gray tone histogram will turn to a unimodal diagram. The droplets at this stage are so called medium drops.
- Big drops: Finally, when the droplets are big enough to reach the steady state condition, the gray tone histogram will have two peaks again, that refer to the drop edges and centers.

C. Drop identification

This last part of the algorithm consists of identifying drops in each image during dropwise condensation in order to determine the evolution of drop characteristics.

1) Very small drops: The very small drops refer to the small elements between pillars(figure 6). The idea of this algorithm is to segment drops by means of correct thresholding values, as shown in figure 7.

At first, in order to eliminating the pillars, they are removed by means of the image generated in the pillar characterization step. Thus, a gray-level image is obtained with black holes at pillar places, as shown in figure 7 (a) and (b). Figure 7 (c) shows the histogram corresponding to the images containing very small droplets. This process is applied in parallel to the first image at time of zero (figure 7 (d), (e) and (f)).

The very small droplets spread the gray tone histogram

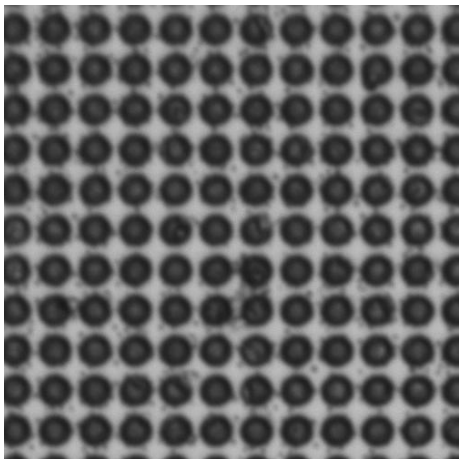

Fig. 6. Image of very small drops on a textured surface

towards darker area, because generally they are darker than the substrate. Therefore, the superposition point between these two histograms can be used as thresholding value for figure 7(a). But since there are lots of superposition points between these two histograms along the vertical axis, the thresholding value can be calculated by finding the superposition point with the maximum value. Figure 7 (g) represents the difference between these two histograms and the zero values in this graph shows the superposition points. So the first zero point after the peak corresponds to the maximum superposition point or the thresholding value. This value then used for thresholding the images containing very small drops as is shown in figure 7 (h). At last each region is labeled according to figure 7 (i). Therefore, the number of regions corresponds to the drop number N, that enables to determine the mean drop radius R_{avg} from the total region area A:

$$R_{avg} = \sqrt{\frac{A_{tot}}{N\pi}}. \quad (1)$$

2) Small drops: Small drops are presented as small circular elements which are smaller than the pillars in the images (figure 8). Since, at this step, droplets are perfectly circular, they can be recognized by means of the Hough transform as shown in figure 9 (b).

Then, as shown in figure 9 (c), the circles corresponding to pillars are removed by comparing the position of circle centers between the considered image and the first image of the set. A binary image is obtained (figure 9 (d)), it gives the total area A_{tot} of drops. To get the number of drops, the overlapping drops need to be separated. For this purpose, the binary image is turned into a distance map by the Euclidean distance (figure 9 (e)) and the watershed technique is applied to this distance map (figure 9 (f)). A labeling step enables to get the drop number and finally, the equation 1 gives the mean radius of drops.

3) Medium drops: The medium drops form a continuous cluster around pillars and drop centers look like background regions (figure 10). Therefore, the centers of drops must be determined by means of some criteria based on both geometry and intensity (figure 11).

In this regard, the original images are firstly thresholded by means of Otsu's method as is shown in figure 11 (b). The problem here is that white area represents both droplets center and substrate. In order to recognising droplets center, two techniques are applied to sufficiently large white regions. The droplets centers are either more convex than substrate or are less homogeneous in intensity. Consequently, the areas with the convexity rate under 4 $\%$ (figure 11 (d)) or with low rate of gradient magnitude refer to the drops centers (figure 11 (c)). The limited rate of gradient magnitude corresponds to 4/5 of the mean gradient magnitude of the neighborhoods. Finally, the binary images of drops as in figure 11 (f) are made by applying the watershed method.

4) Big drops: Big drops are characterized by the fact that they cover entirely several pillars as shown in figure 12. For binarizing images containing big droplets, shrinking and gradient properties are used (figure 13).

Firstly, the images are thresholded by a Otsu's method as shown in figure 13 (b). Then, the black parts are shrunk in order to get their skeletons (figure 13 (c)) around the white regions which correspond to either drops centers or the background. As was explained for the medium drops, the average of gradient magnitude is calculated on the white regions according to figure 13 (d). Then, the distribution of this value is divided into two groups by means of the histogram specification, the median between the two main peaks, that gives the criterion value (figure 13 (e)).

However, when several white regions belong to the same drop, the watershed technique can't be applied directly. To solve this problem, the white regions are dilated and overlaid with the pillar image. Thus, the white regions which belong to the same drop are connected. A test on convexity enables to reconstruct each drop center (figure 13 (g)). Finally, a watershed technique is used to detect each drop region (figure 13 (h)), that enables to get the drops number and mean radius.

IV. Algorithm verification

In order to measure quantitatively the performance of this algorithm, the drops are divided into four groups according to their presence in the initial configuration and their detection by the algorithm:

- The true positive drops (TP) which are detected by the algorithm and are present in the initial image.
- The false positive drops (FP) which are detected by the algorithm but are not present in the initial image.
- The false negative drops (FN) which are not detected by the algorithm but are present in the initial image.

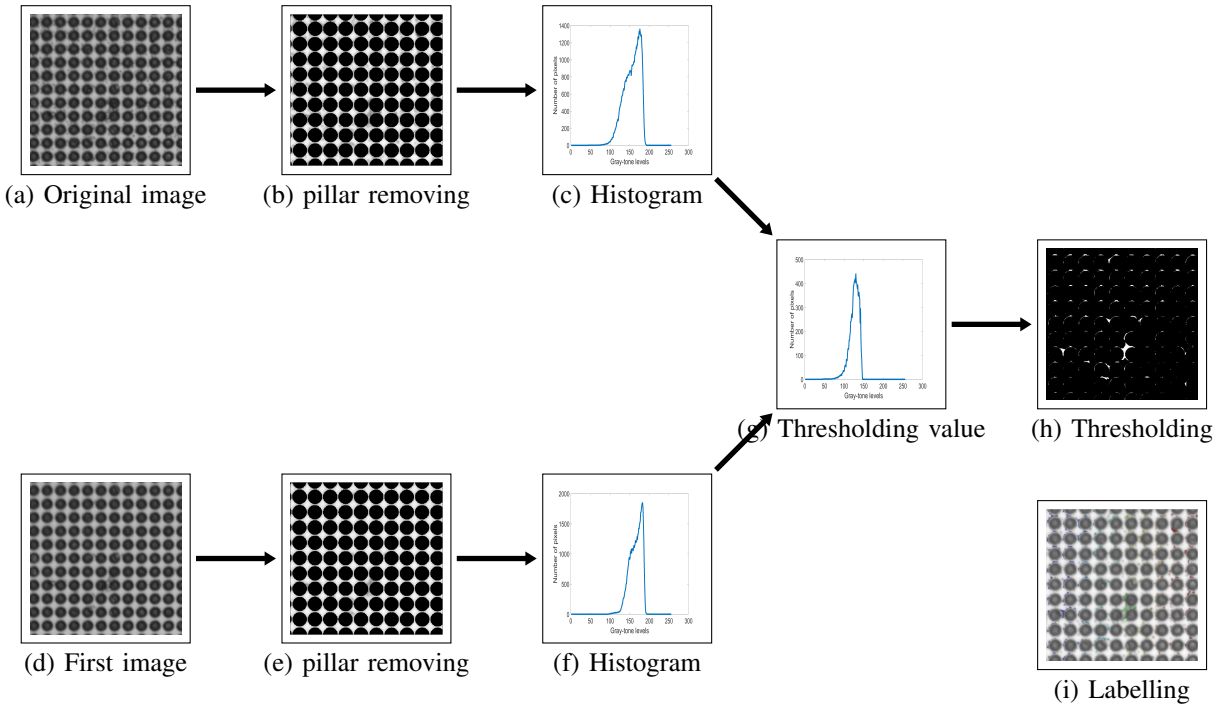

Fig. 7. Algorithm for very small drops

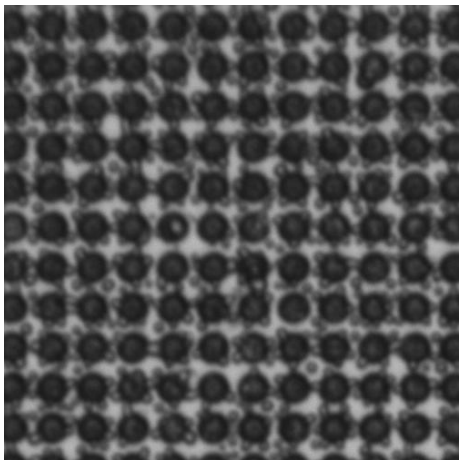

Fig. 8. Image of small drops on a textured surface

- The true negative drops (TN) which are not detected by the algorithm and are not present in the original image.

The number of drops which belong to each groups enables to estimate the precision (PR) and the recall (RC) of the algorithm:

$$PR = \frac{TP}{TP + FP}, \tag{2}$$

$$RC = \frac{TP}{TP + FN}. \tag{3}$$

A high value of PR indicates that detected drops are present in the original image and there can be other drops which are not detected by the algorithm. On the contrary, a high value of RC indicates that the algorithm detects almost all drops, but it also detects some drops, which do not exist in the original image. Thus, these both measurements suffer from a lack of accuracy. In fact, neither FN nor FP are not preferred for an accurate algorithm. That's why, a more robust measurement of the algorithm accuracy so-called F-measure (FM) is used [30]:

$$FM = \frac{2}{1/PR + 1/RC}. \tag{4}$$

In order to evaluate the F-measure of this algorithm, the drops are manually detected in a sub-sampling of images and are compared with those detected by means of the algorithm. This study is led to two kinds of surfaces (grid pattern and quincunx pattern) in order to determine the application conditions of the algorithm. Table I shows the evolution of the F-measure as a function of the considered image set and the drop size.

The low values obtained for small drops can be explained by the fact that drops are not really circular because they are adjacent to pillars. Despite these mismeasurements, Table I shows that this algorithm is very accurate, especially for large drops. Although the detection on the quincunx pattern is less accurate. Thus, the pillar pattern has an influence on the algorithm accuracy.

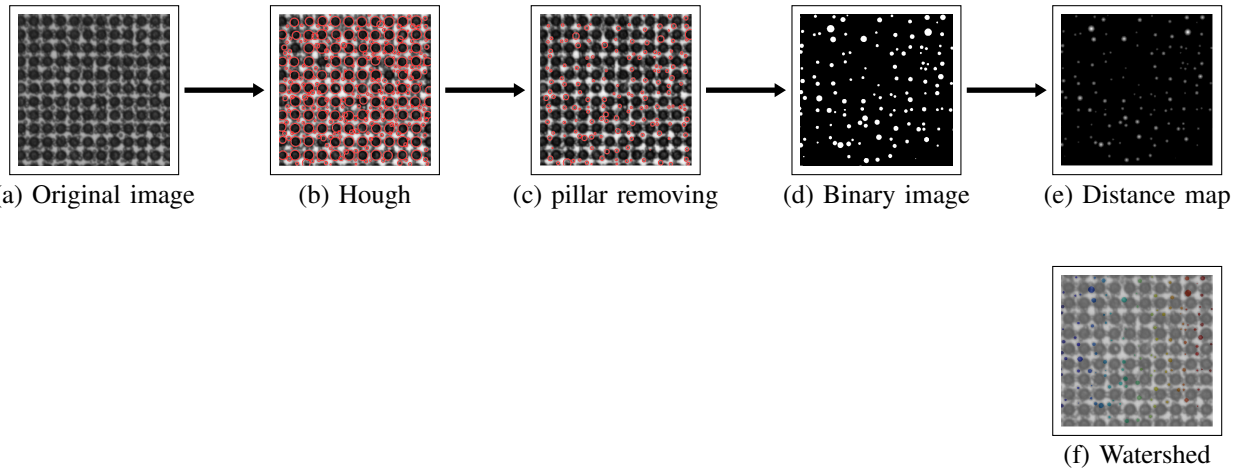

(a) Original image (b) Hough (c) pillar removing (d) Binary image (e) Distance map

(f) Watershed

Fig. 9. Algorithm for small drops

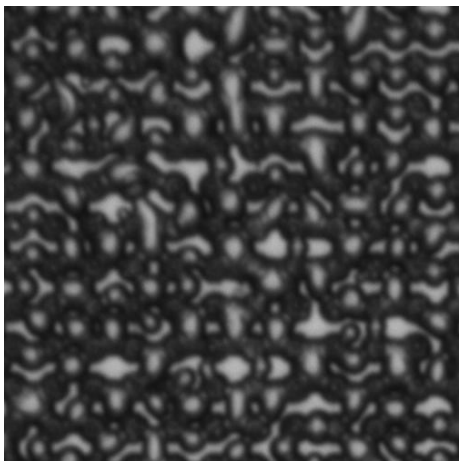

Fig. 10. Image of medium drops on a textured image

Set	Drop size	FM
Regular pattern	Very small	75 %
	Small	49 %
	Medium	84 %
	Big	93 %
Quincunx	Very small	-
	Small	5 %
	Medium	71 %
	Big	87 %

TABLE I
PERFORMANCE PARAMETERS OF THE ALGORITHM FOR SEVERAL IMAGE SETS

V. APPLICATION TO TEXTURED SURFACES

The developed image processing algorithm is applied to images generated by the experimental set-up described in Section 2. Several texturation are tested: grid pattern and quincunx pattern.

Figure 14 shows the evolution of the drop mean radius during dropwise condensation for both textured surfaces. The measurements were done every $10s$ in order to reduce the computational time. As can be seen in this figure, the drops mean radius increases to reach a steady state situation, that follows the theory of dropwise condensation: droplets grow and coalesce until reaching a regular pattern [5].

Figure 15 shows the evolution of the drop number during dropwise condensation for both of the textured surfaces. In both cases, the drops number decreases rapidly to reach a steady state situation, after which the number of droplets follow a constant pattern.

The steady state situation in both radius and number of droplets is due to coalescence phase, during which two or more small droplets merge and form a bigger droplet. This phenomenon leads to decrease in the total surface area covered by the droplets, In the vacant area formed after coalescence new small droplets can nucleate continuously. The opposite effect of coalescence and nucleation of new small droplets on the average size and total number of droplets will lead to an approximately constant pattern in these two diagrams.

However, the fluctuations at the initial seconds of the algorithm show the lack of robustness of this algorithm in initial stages of dropwise condensation.

The comparison between droplets radius and density between two kinds of texturation reveals that, the drops mean radius for the quinqunx pattern is lower than the one for the grid pattern. In parallel, the initial droplets density for the grid pattern is higher than quinqunx pattern. While for both texturations, these measurements reach the same values at steady state: $0.25mft$ for the mean radius and $301/ft^2$.

Figure 16 and 17 compare the drop characteristics of the grid patterned surface with a flat surface formed with the same material in order to see the influence of pillars on the drop evolution. According to figure 16, the presence

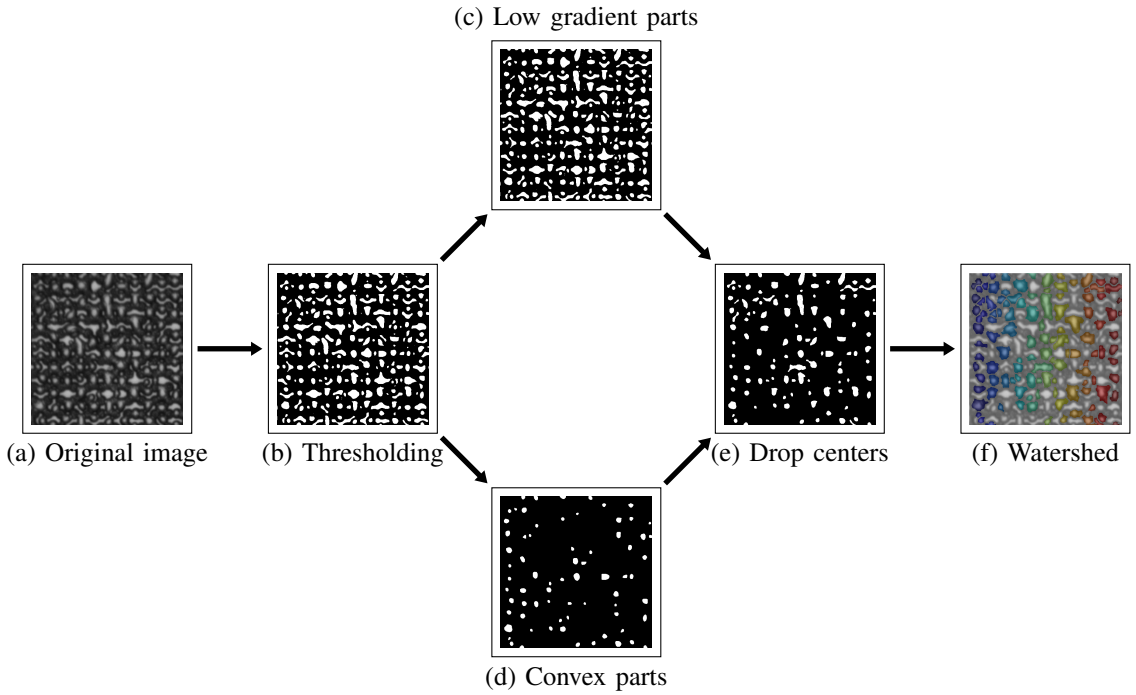

Fig. 11. Algorithm for medium drops

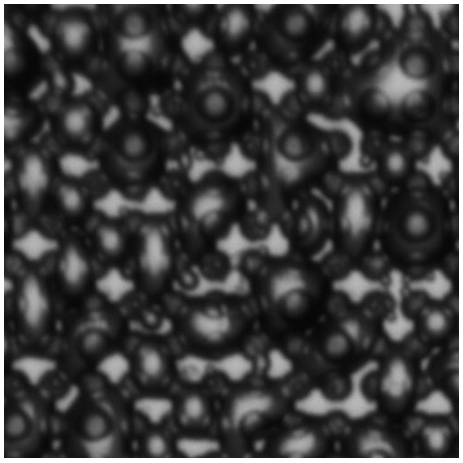

Fig. 12. Image of big drops on a textured image

of the pillars limits the increasing of drop radius at steady state of about 50%. However, during other steps, droplets on the flat surface are respectively larger. On the other hand, the presence of pillars increases considerably the drops number during the initial steps.

VI. Conclusion

A robust image processing algorithm has been developed for drop measurement on textured surfaces. The existing techniques of drop measurement have been discussed and have been proved to be adequate in the case of pillar texturation too. Thus, the developed algorithm combines the geometrical, optical and topological information of the images to segment the droplets. It is capable of segmenting drops with a large range of radius. Indeed, by means of an histogram analysis, it can estimate the drop size, divides the drops in four main size range and uses a corresponding algorithm adapted to each size range. A manual verification of drop detection ability of the present algorithm comparing to real images is conducted to verify the algorithm accuracy. The F-measure enables to quantify the accuracy of the detection and to show that this algorithm has a high accuracy for drops with a radius over $0.15mft$.

The developed algorithm gives the evolution of drops mean radius and number per unit area during dropwise condensation. It has been applied to two kinds of textured surfaces in order to compare the wettability of each texturation. This comparison shows that the texturation pattern affects the droplets size and the density before steady state situation. The comparison with flat surface shows that, although texturation enables to reduce the droplets size at later stages , it increases the density of initial nucleation.

ACKNOWLEDGMENT The authors would like to thank Nicolas Pionnier for the experimental results obtained during his PhD funded by PSA Peugeot-Citroen in the context of OpenLab VATLyon between Peugeot-Citroen and LTDS laboratory. This work was funded by LABEX MANUTECH-SISE (ANR-10-LABX-0075,

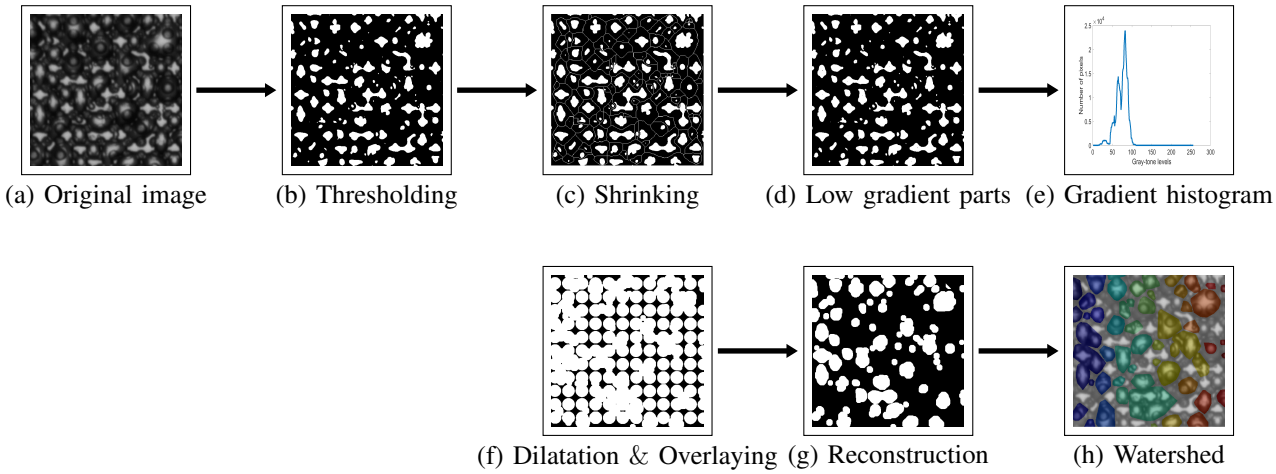

Fig. 13. Algorithm for big drops

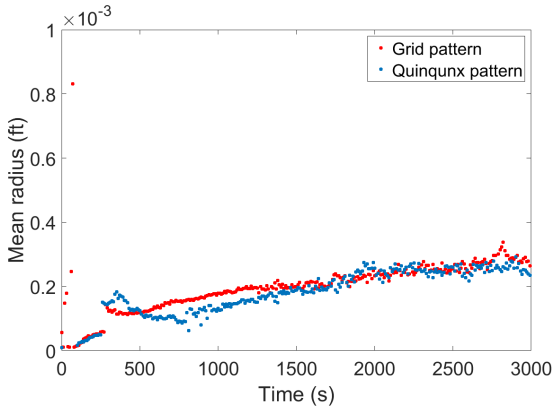

Fig. 14. Evolution of the mean radius as a function of time for two kinds of texturation

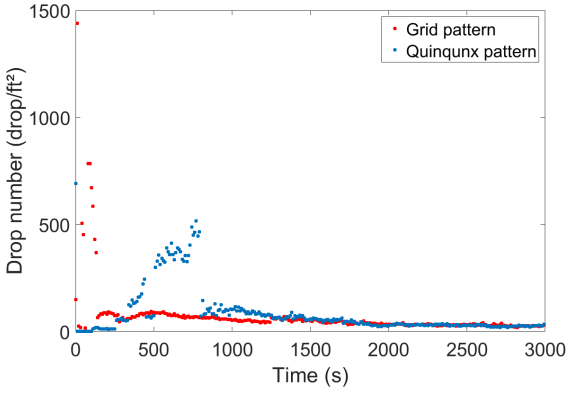

Fig. 15. Evolution of the drops number as a function of time for two kinds of texturation

within the program ”Investissements dAvenir” (ANR-11-IDEX-0007) operated by the French National Research Agency (ANR).

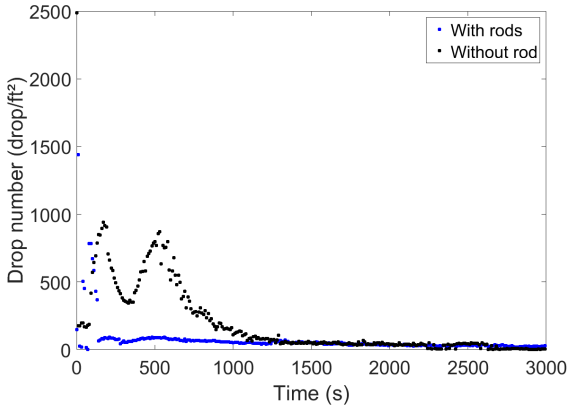

Fig. 16. Comparison of the mean radius evolution for a grid patterned surface and a flat surface

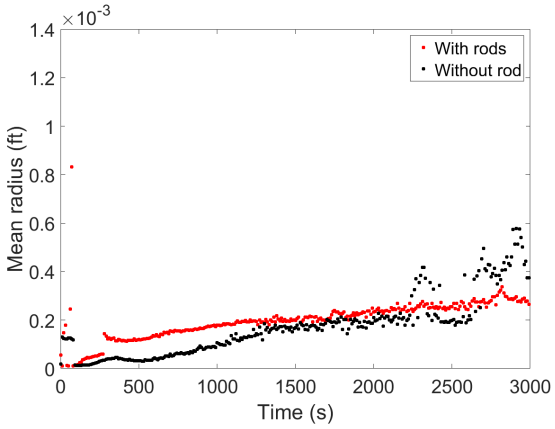

Fig. 17. Comparison of the drop number evolution for a grid patterned surface and a flat surface

REFERENCES

[1] RN Leach, F Stevens, SC Langford, and JT Dickinson. Dropwise condensation: experiments and simulations of nucleation and

growth of water drops in a cooling system. *Langmuir*, 22(21):8864–8872, 2006.

[2] A Cengel Yunus et al. Heat transfer: a practical approach. *MacGraw Hill, New York*, 2003.

[3] Julian E Castillo, Justin A Weibel, and Suresh V Garimella. The effect of relative humidity on dropwise condensation dynamics. *International Journal of Heat and Mass Transfer*, 80:759–766, 2015.

[4] RN Leach, F Stevens, SC Langford, and JT Dickinson. Dropwise condensation: experiments and simulations of nucleation and growth of water drops in a cooling system. *Langmuir*, 22(21):8864–8872, 2006.

[5] JW Rose and LR Glicksman. Dropwise condensationthe distribution of drop sizes. *International Journal of Heat and Mass Transfer*, 16(2):411–425, 1973.

[6] Basant Singh Sikarwar, Sameer Khandekar, and K Muralidhar. Mathematical modelling of dropwise condensation on textured surfaces. *Sadhana*, 38(6):1135–1171, 2013.

[7] Yucheng Fu and Yang Liu. Development of a robust image processing technique for bubbly flow measurement in a narrow rectangular channel. *International Journal of Multiphase Flow*, 84:217–228, 2016.

[8] Soo-Chang Pei and Ji-Hwei Horng. Circular arc detection based on hough transform. *Pattern recognition letters*, 16(6):615–625, 1995.

[9] Xiaoran Yu, Dongchang Xing, Tatsuya Hazuku, Tomoji Takamasa, Takashi Ishimaru, Yuji Tanaka, and Tatsuro Akiba. Measurement technique for solid-liquid two-phase flow using a normal-line hough transform method. In *Journal of Physics: Conference Series*, volume 147, page 012053. IOP Publishing, 2009.

[10] TJ Atherton and DJ Kerbyson. Using phase to represent radius in the coherent circle hough transform. In *Hough Transforms, IEE Colloquium on*, pages 5–1. IET, 1993.

[11] N Senthilkumaran and R Rajesh. Edge detection techniques for image segmentation–a survey of soft computing approaches. *International journal of recent trends in engineering*, 1(2):250–254, 2009.

[12] Liping Shen, Xiangqun Song, Manabu Iguchi, and Fujio Yamamoto. A method for recognizing particles in overlapped particle images. *Pattern Recognition Letters*, 21(1):21–30, 2000.

[13] Markus Honkanen et al. Turbulent multiphase flow measurements with particle image velocimetry: application to bubbly flows. 2002.

[14] Herbert Freeman and Larry S. Davis. A corner-finding algorithm for chain-coded curves. *IEEE Transactions on computers*, 26(3):297–303, 1977.

[15] Cristina Urdiales, Antonio Bandera, and F Sandoval. Non-parametric planar shape representation based on adaptive curvature functions. *Pattern Recognition*, 35(1):43–53, 2002.

[16] R Lindken and W Merzkirch. A novel piv technique for measurements in multiphase flows and its application to two-phase bubbly flows. *Experiments in fluids*, 33(6):814–825, 2002.

[17] Serge Beucher and Fernand Meyer. The morphological approach to segmentation: the watershed transformation. *Optical Engineering-New York-Marcel Dekker Incorporated-*, 34:433–433, 1992.

[18] X Zabulis, M Papara, A Chatziargyriou, and TD Karapantsios. Detection of densely dispersed spherical bubbles in digital images based on a template matching technique: Application to wet foams. *Colloids and Surfaces A: Physicochemical and Engineering Aspects*, 309(1):96–106, 2007.

[19] Andrew Fitzgibbon, Maurizio Pilu, and Robert B Fisher. Direct least square fitting of ellipses. *IEEE Transactions on pattern analysis and machine intelligence*, 21(5):476–480, 1999.

[20] Tomislav Marošević and Rudolf Scitovski. Multiple ellipse fitting by center-based clustering. *Croatian Operational Research Review*, 6(1):43–53, 2015.

[21] Antonio LaTorre, Lidia Alonso-Nanclares, Santiago Muelas, JM Peña, and Javier DeFelipe. Segmentation of neuronal nuclei based on clump splitting and a two-step binarization of images. *Expert Systems with Applications*, 40(16):6521–6530, 2013.

[22] WX WONG and O Stephansson. Binary image segmentation of aggregates based on polygonal approximation. In *Scandinavian conference on image analysis*, pages 709–716, 1997.

[23] D Thompson, H Bartels, J Haddad, and P Bartels. Scene segmentation in a machine vision system for histopathology. *SPIE J*, 1206:40–47, 1990.

[24] SH Ong, HH Yeow, R Sinniah, et al. Decomposition of digital clumps into convex parts by contour tracing and labelling. *Pattern Recognition Letters*, 13(11):789–795, 1992.

[25] Ashish Karn, Christopher Ellis, Roger Arndt, and Jiarong Hong. An integrative image measurement technique for dense bubbly flows with a wide size distribution. *Chemical Engineering Science*, 122:240–249, 2015.

[26] Qing Chen, Xiaoli Yang, and Emil M Petriu. Watershed segmentation for binary images with different distance transforms. In *Proceedings of the 3rd IEEE International Workshop on Haptic, Audio and Visual Environments and Their Applications*, pages 111–116, 2004.

[27] Robert M Haralick and Layne Watson. A facet model for image data. *Computer Graphics and Image Processing*, 15(2):113–129, 1981.

[28] Timo Ojala, Matti Pietikainen, and David Harwood. Performance evaluation of texture measures with classification based on kullback discrimination of distributions. In *Pattern Recognition, 1994. Vol. 1-Conference A: Computer Vision & Image Processing., Proceedings of the 12th IAPR International Conference on*, volume 1, pages 582–585. IEEE, 1994.

[29] Kuen-Long Lee, Ling-Hwei Chen, et al. A new method for coarse classification of textures and class weight estimation for texture retrieval. *Pattern Recognition and Image Analysis C/C of Raspoznavaniye Obrazov I Analiz Izobrazhenii*, 12(4):400–410, 2002.

[30] Tom Fawcett. An introduction to roc analysis. *Pattern recognition letters*, 27(8):861–874, 2006.